Research Article | Vol. 27, No. 3 | 4 Feb 2019 | OPTICS EXPRESS 2317
Optics EXPRESS

Terahertz electric field modulated mode coupling in graphene-metal hybrid metamaterials

SHAOXIAN LI,[1,2,3] PRIYO S. NUGRAHA,[2,3] XIAOQIANG SU,[1,4] XIEYU CHEN,[1] QUANLONG YANG,[1] MÁRTA UNFERDORBEN[5], FERENC KOVÁCS[6], SÁNDOR KUNSÁGI-MÁTÉ[2,6,7], MENG LIU,[1] XUEQIAN ZHANG,[1] CHUNMEI OUYANG,[1,*] YANFENG LI,[1] JÓZSEF A. FÜLÖP,[2,3,8] JIAGUANG HAN,[1] AND WEILI ZHANG[1,9]

[1]*Center for Terahertz Waves and College of Precision Instrument and Optoelectronics Engineering, and the Key Laboratory of Optoelectronics Information and Technology, Ministry of Education, Tianjin University, Tianjin 300072, China*
[2]*Szentágothai Research Centre, University of Pécs, Ifjúság ú. 20, 7624 Pécs, Hungary*
[3]*MTA-PTE High-Field Terahertz Research Group, Ifjúság ú. 6, 7624 Pécs, Hungary*
[4]*Institute of Solid State Physics, Shanxi Datong University, Datong 037009, China*
[5]*Institute of Physics, University of Pécs, Ifjúság ú. 6, 7624 Pécs, Hungary*
[6]*Department of General and Physical Chemistry, University of Pécs, Ifjúság útja 6, 7624 Pécs, Hungary*
[7]*Department of Pharmaceutical Chemistry, University of Pécs, Rókus u. 2, H-7624 Pécs, Hungary*
[8]*ELI-ALPS, ELI-Hu Nonprofit Ltd., Dugonics tér 13, 6720 Szeged, Hungary*
[9]*School of Electrical and Computer Engineering, Oklahoma State University, Stillwate, Oklahoma 74078, USA*
**cmouyang@tju.edu.cn*

Abstract: Taking advantage of the tunable conductivity of graphene under high terahertz (THz) electric field, a graphene-metal hybrid metamaterial consisting of an array of three adjoined orthogonally oriented split-ring resonators (SRRs) is proposed and experimentally demonstrated to show a maximum modulation depth of 23% in transmission when the THz peak field reaches 305 kV/cm. The transmission of the sample is dominated by the antisymmetric and symmetric resonant modes originating from the strong magneto-inductive and conductive coupling among the three SRRs, respectively. Numerical simulations and model calculations based on a coupled oscillator theory were performed to explain the modulation process. It is found that the graphene coating impairs the resonances by increasing the damping of the modes and decreasing the coupling between the SRRs whereas the strong THz field restores the resonances by decreasing the conductivity of graphene.

1. Introduction

Metamaterials offer unprecedented ways to manipulate light [1,2]. Owing to the conveniently long wavelength, functional metamaterials have been extensively studied and utilized in the terahertz (THz) band [3,4]. The coupling between the structural units of metamaterials play a key role in determining their properties and performance [5,6]. One example is electromagnetically induced transparency (EIT), realized by the coupling between the bright mode and the dark mode in metamaterials [7–10]. Moreover, mode coupling between metamaterials and natural materials is possible [11,12] and metamaterials usually are sensitive to their surroundings [13,14]. This opens a way to design active metamaterials, advantageous for many practical applications. Metamaterials integrated with semiconductor, superconductor and phase changing materials have been demonstrated to have a good tunability [15–22]. Recently, the remarkable photoconductivity of organic–inorganic lead halide perovskites was exploited to realize extremely low power photoswitching of the

#347946 https://doi.org/10.1364/OE.27.002317
Journal © 2019 Received 11 Oct 2018; revised 26 Dec 2018; accepted 27 Dec 2018; published 25 Jan 2019

Optics EXPRESS

metamaterial resonances in the THz band [23]. Mode coupling due to the interaction of the Fano resonance with the optically active phonon mode of the perovskite sample was observed. By pumping a similar asymmetric split ring array with a 310 nm thick germanium coating at 1200 mW, an ultrafast all-optical switching was demonstrated to show a resonant transmission modulation depth of 90% and a full recovery time of 17 ps [24]. Another approach to manipulate mode coupling and obtain good modulation is micro/nano electromechanical systems (MEMS/NEMS) metamaterials. Manjappa and coauthors demonstrated a reconfigurable MEMS Fano metasurface with multiple-input–output states for logic operations at terahertz frequencies [25]. By controlling the released heights of two split ring resonators cantilever arms independently, the out-of-plane structural asymmetry is tuned to modify the near-field coupling of the resonators directly. A change of 61% in transmittance at 0.56 THz was demonstrated at the maximum out-of-plane structural.

Graphene is a two-dimensional material and its conductivity can easily be tuned by electric gating and optical doping. Good modulation of transmission and reflection has been achieved by graphene on substrate [26–28]. Though significant efforts have been devoted to various designs of graphene-based metamaterials utilizing the tuning of the conductivity of graphene by electric gating [29,30], only a few experiments have been reported in the THz band [31–34]. Kim and coauthors demonstrated an electrically tunable graphene EIT metamaterial and achieved a very large group delay modulation up to 3.3 ps with low gate voltage [35]. The electric control of EIT effect is realized by tuning the damping rate of the dark resonance by varying the optical conductivity of the graphene layer. Using a similar strategy but with a patterned graphene covering the gap of C-shaped metal resonator, Kindness and coauthors presented an active EIT metamaterial which can readily be implemented as an electronic tunable band pass/reject filter with a tuning range of ~100 GHz operating at 1.5 THz [36]. In addition to the interplay between graphene and coupled resonator arrays, graphene can create electrical interconnections between metallic unit structures of metamaterials. Jung and coauthors reported that the resonance frequency of the terahertz metamaterials can be tuned as a function of the number of connected units [37]. The voltage-controlled connections allow delicate control over the phase shift of the transmitted THz field, without changing the high transmission. Until now, most of the designs and experiments about graphene-metal hybrid metamaterials were carried out in the frame of linear interaction with THz waves, i.e. working under low THz electric field. Under high THz electric field, the conductivity of graphene can be tuned [38–40], which gives another opportunity to design active metamaterials.

In this work, we present a study of a THz electric field dependent nonlinear metamaterials consisting of an array of three adjoined orthogonally oriented split resonant rings (SRRs) coated with monolayer graphene. A maximum modulation depth of 23% in transmission has been experimentally achieved with up to 305 kV/cm THz peak field. Simulations and model calculations have been performed and it is found that the mechanism behind the modulation is the graphene tuned coupling and damping of the modes in the metamaterials under different THz electric field strength. Our study can be useful for future designs of graphene hybrid metamaterials working under high THz electric field.

2. Experimental results and discussion

A graphene-metal hybrid metamaterial has been fabricated, where the transmission is dominated by the strong electromagnetic coupling. As shown in Fig. 1(a), it contains a periodic metal pattern on top of a 450 μm thick sapphire. The size of the unit cell (P) is 100 μm by 100 μm and the size of the whole sample is 1 cm by 1 cm. Each unit cell contains a three-split-ring structure made of aluminum. The left and right SRRs are rotated in opposite directions by 90° with respect to the middle one. One side of each SRR is shared with its neighbor. The side length of the individual rings is L = 28 μm, the strip width is w = 3 μm, and the split gap is d = 4 μm wide. The thickness of the metal pattern layer is 200 nm. Finally,

Optics EXPRESS

a monolayer graphene has been transferred on top of the metal pattern layer using wet-transferring methods [41]. Raman spectra were measured with a 633 nm pump photoexcitation to characterize the graphene layer in the gaps and other areas around the SRRs in the metamaterial. A typical Raman spectrum is illustrated in Fig. 1(b). The experimental data (dashed lines) are fitted with Lorentz curves (solid lines). The peak positions of the G and G' modes, the spectral width of the G' mode and the peak intensity ratio of G' mode to G mode agree with the study by Liu et al. [42]. The spectral width of the G mode in our experiment was about 10.8 cm^{-1} which is smaller than 15 cm^{-1} reported in literature [42]. This deviation may come from the hole doping [43]. The Raman spectrum clearly shows that the monolayer graphene could be transferred to the metamaterial surface.

The linear THz transmission spectrum of the sample before and after transferring of the monolayer graphene were measured using a commercial time-domain THz spectrometer (Menlo Systems). For characterizing the THz field strength dependent transmission of the sample, a home-built strong-field THz spectrometer, available at University of Pécs, has been used. Intense THz pulses have been generated in a $LiNbO_3$ crystal using tilted-pulse-front pumping [44]. Pump pulses of 1030 nm central wavelength, 200 fs pulse duration, and 1 kHz repetition rate have been used. A reflective grating and an achromatic lens were used to generate the required pulse front tilt of 63° in the crystal [45]. The emitted THz pulses were collimated and focused by a 4-inch focal length 90° off-axis parabolic (OAP) mirror and a 2-inch focal length OAP mirror, respectively. In the focal plane, a THz spot with a spot size of 1.84 mm by 1.58 mm and energy of 4.65 μJ was obtained when the $LiNbO_3$ crystal was pumped by 3.2 mJ laser pulses. The sample was placed in the focal plane to facilitate interaction with the highest THz field strength. The modulated THz pulses, transmitted through the sample, were collimated by a 3-inch focal length OAP mirror and focused to the ZnTe detector crystal by a 4-inch focal length OAP mirror. The ZnTe detector crystal consisted of an <110>-cut effective layer of 0.1 mm thickness, and a 2 mm thick ineffective <100>-cut ZnTe substrate. Based on the measured THz spot size, pulse energy, and waveform, the peak electric field at the sample position was estimated to be 305 kV/cm [46]. The polarization of the THz electric field incident on the sample was fixed to be along the long side of the three adjoined SRRs and the field strength was varied by two wire-grid polarizers placed between the first and second OAP mirrors.

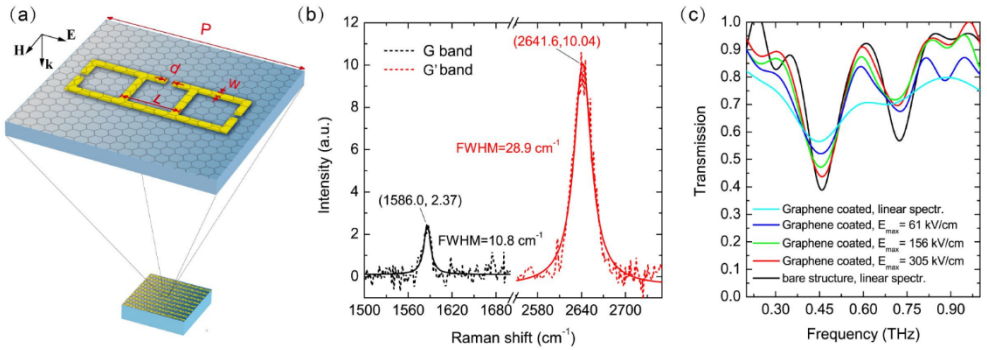

Fig. 1. (a) Schematic of the graphene-metal hybrid metamaterial, with geometric parameters P = 100 μm, L = 28 μm, w = 3 μm, and d = 4 μm. (b) Measured Raman spectrum of monolayer graphene around the SRRs on the sapphire substrate. (c) Measured transmission spectra of the sample with and without graphene coating under different THz field strengths.

Figure 1(c) shows the THz transmission of the sample under different conditions. As shown by the black line, the uncoated metamaterial sample exhibits two resonances at 0.45 THz and 0.7 THz, respectively. When coated by the monolayer graphene, both resonances become weak; the transmission at 0.45 THz and 0.7 THz increases from 0.38 to 0.55 and from 0.57 to 0.7, respectively. The high-transmission window between the two resonances

Optics EXPRESS

shows a transmission decrease from 0.92 to 0.71 at around 0.6 THz. The weakening of the resonances is caused by the increased damping of the resonant modes and the reduced coupling between the three SRRs. The middle SRR can be excited by the external E-field directly and then transfer energy to the left and right SRRs. As will be shown in more detail in Section 3, the two resonances, corresponding to antisymmetric and symmetric modes, arise from the magneto-inductive and the conductive coupling between the three SRRs, respectively [47,48]. The resonances of the two outer SRRs can couple back to the middle SRR. SRRs can be very sensitive to the graphene coating because the graphene can shortcut the gap and decrease the resonator's Q factor [13]. In addition, the weaker response of the middle SRR to the external THz field and the increased damping of the resonances in the three SRRs impairs the coupling between them. However, when increasing the THz electric field, the observed transmission gradually approached that of the uncoated sample, as clearly shown by the spectra measured at 61 kV/cm, 165 kV/cm, and 305 kV/cm in Fig. 1(c). The restoring of the resonances is due to the lower conductivity of graphene under higher THz electric field, thus having less effect on the resonances.

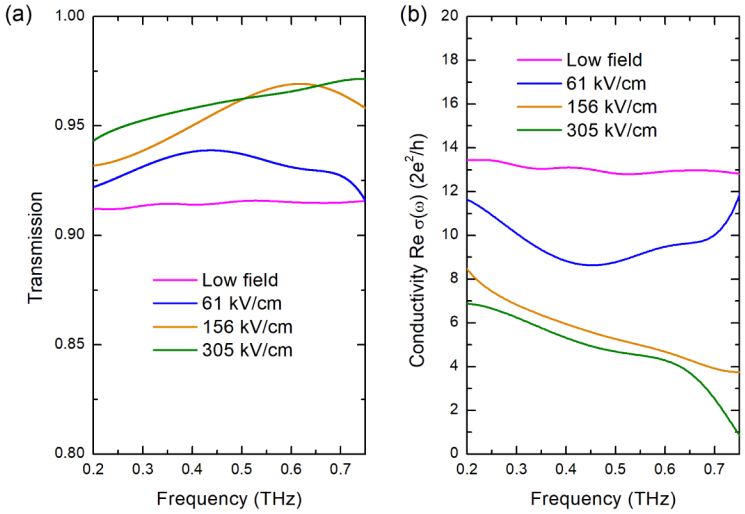

Fig. 2. (a) Measured THz transmission of monolayer graphene on the sapphire substrate at different THz field strengths. (b) Real part of the conductivity of graphene, obtained from the transmission measurements in (a).

In order to support this explanation in experiment, the THz transmission of the sapphire substrate coated by monolayer graphene has also been measured at various THz electric field strengths. The bare sapphire substrate was used as reference. As shown in Fig. 2(a), about 4% increase in the transmission was observed when the THz field increased from a low value to 305 kV/cm. The observed trend agrees with those reported in the literature [38–40]. The transmission of graphene can be described by the formula $t = (1+n_{sapp})/(1+n_{sapp}+Z_0\sigma_g)$, where $t, n_{sapp}, Z_0, \sigma_g$ are the THz transmission of graphene, the refractive index of the sapphire substrate, the wave impedance in free space, and the sheet conductivity of monolayer graphene, respectively [49]. Figure 2(b) shows the real part of the conductivity of graphene, extracted from the transmission spectra. It clearly shows the decreasing conductivity of graphene as the THz field strength increases.

3. Simulation and model analysis

To understand the magneto-inductive coupling and the conductive coupling in the three SRRs, the transmissions of single SRRs, double SRRs and three SRRs were simulated using

Optics EXPRESS

the software CST Microwave Studio. As shown in Fig. 3, the single SRR structure exhibits a single resonance at 0.7 THz. When a 90°-rotated second SRR was attached, to form a double SRR, two resonant modes appear. The circular currents excited in each of the two joint SRRs oscillate out-of-phase and in-phase at the low-frequency mode and the high-frequency mode, respectively. Consequently, the magnetic dipole moments of the constituent rings are aligned antiparallel and parallel to each other, respectively, which is also obvious from the distribution of the magnetic field component perpendicular to the plane of the structure. For three SRRs, the magnetic field distribution in the left and right SRRs are symmetric to the middle SRR and exhibit common resonance behavior, which helps to enhance the coupling between the middle SRR. This strong coupling leads to a red-shift of the low-frequency mode and the increase of the resonance strengths of both modes. For the high-frequency mode, because the currents from the connecting part contribute oppositely for the three SRRs, no significant shift of the resonance frequency occurs [47,48].

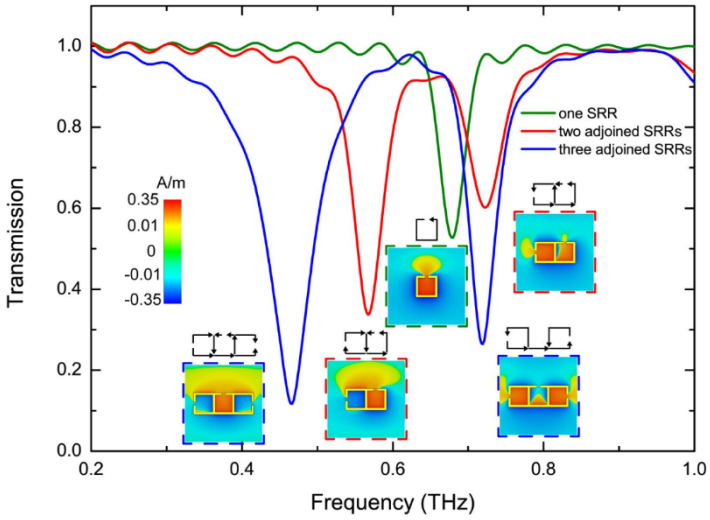

Fig. 3. Simulated THz transmission of uncoated metamaterials with single SRR, double SRRs, and three adjoined SRRs in the unit cell, along with current directions and normal magnetic field component distributions at resonances.

To study the THz-field dependent effect of graphene on the coupling in the three SRRs, the THz transmissions, surface currents, and electric field distributions have been simulated assuming different values for graphene conductivity. As shown in Fig. 4(a), with decreasing conductivity of graphene by decreasing scattering time, the resonances of the two modes are enhanced and the transmission spectra evolve towards the one without graphene coating. The simulated transmission spectra agree with the experimental results qualitatively. The corresponding conductivity of graphene used in the simulation is shown in Fig. 4(b). In the simulation, it is assumed that the scattering time τ = 25 fs at low THz field, which is a reasonable value regarding to the reported values in literature [34,35,50,51]. τ decreases with the increase of the THz field strength, which is consistent with the arguments in literature [39,52]

Optics EXPRESS

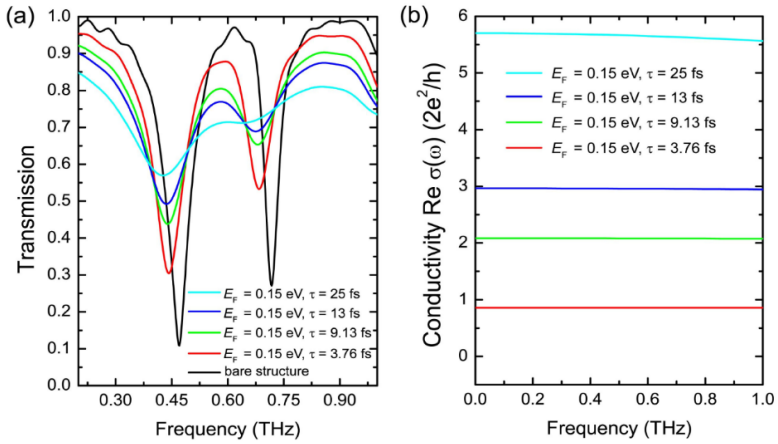

Fig. 4. (a) Simulated THz transmissions of the sample without and with graphene coating. The conductivity of graphene is tuned by varying the scattering time. (b) The real part of conductivity of graphene used in the simulation.

Figure 5(a) shows the typical surface currents for the low-frequency mode (mode 1), the transmission window (0.6 THz), and the high-frequency mode (mode 2) for uncoated sample. For the transmission window at 0.6 THz, the surface current is weak as compared to those for the two modes. Therefore, the resonances in the three SRRs are weak and lead to a high transmission. At this transmission window, there is a phase retardation of the surface currents in the left and right SRRs with respect to the middle SRR. Thus, during one period, the magnetic dipole moment of each SRR can be opposite to the one that is beside it at one time and all the magnetic dipole moments have the same orientation at the other time. This phenomenon demonstrates that hybridization or interference between the low-frequency mode and high-frequency mode occurs in the transmission window. The root-mean-squared electric field amplitude distribution at the low-frequency mode, 0.6 THz, and high-frequency mode near the three SRRs are shown in Fig. 5(b). Without graphene on the SRRs, strong localized electric fields are observed in the gaps of the SRRs. Once the graphene was coated, the localized electric fields become weak, as shown in the column corresponding to E_F = 0.15 eV and τ = 25 fs. This is due to the fact that graphene with high conductivity in the gaps tend to shortcut the SRRs circuit and increase the damping of the resonant modes. When graphene is interacted with high THz electric field, its conductivity is decreased and the shorting effect weakens. The localized electric fields in the gaps increase as shown in the column corresponding to E_F = 0.15 eV and τ = 9.13 fs.

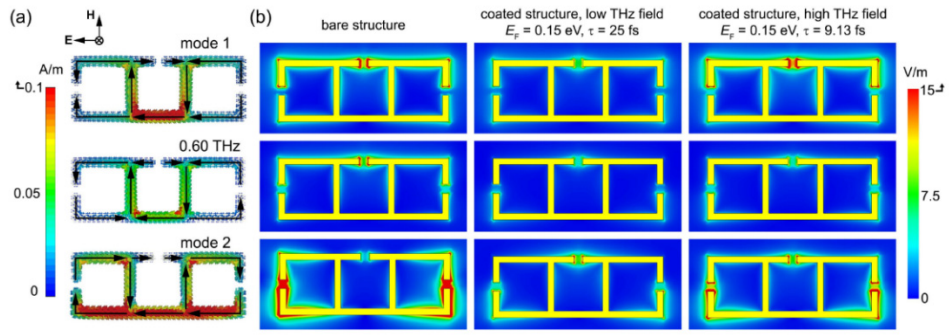

Fig. 5. (a) Surface currents at the two resonances and in the transmission window (0.6 THz) of the sample without graphene coating. (b) Corresponding distributions of the root-mean-squared electric field amplitudes of the metamaterial without graphene coating and coated with graphene with different conductivity.

Optics EXPRESS

To further study the effect of graphene on the coupling and damping rate of resonant modes, an analytical model based on the coupled oscillator theory is used to describe the transmission spectra obtained in the experiment. Equations (1) and 2 describe the oscillations of the middle ring and the two side rings, respectively [7].

$$\ddot{x}_1 + \gamma_1 \dot{x}_1 + \omega_1^2 x_1 + \kappa_{12} x_2 = g \times E\,, \tag{1}$$

$$\ddot{x}_2 + \gamma_2 \dot{x}_2 + \omega_2^2 x_2 + \kappa_{12} x_1 = 0\,. \tag{2}$$

The parameters γ_i and ω_i are the damping rates and the eigen frequencies (i = 1,2), respectively. The parameter κ_{12} is introduced to describe the coupling between the two oscillators and the parameter g defines the coupling between the external THz electric field and the middle ring. Because the unit cell is much smaller than the resonant THz wavelength, we can consider the metamaterial layer as an effective medium. The susceptibility χ_e of each unit can be expressed as [19]:

$$\chi_e = \frac{g \times (-\omega^2 + i\gamma_2\omega + \omega_2^2)}{(-\omega^2 + i\gamma_1\omega + \omega_1^2) \times (-\omega^2 + i\gamma_2\omega + \omega_2^2) - \kappa_{12}^2}\,. \tag{3}$$

The transmission of the metamaterial layer can be described by the formula:

$$T = \left| \frac{c(1+n_{sapp})}{c(1+n_{sapp}) - i\chi_e} \right|, \tag{4}$$

where c is the light velocity in vacuum and n_{sapp} = 3.08 is the refractive index of the sapphire substrate [19]. The calculation results, shown in Fig. 6(a), are in good agreement with the experiment data. From the fitting parameters (see Fig. 6(b)), one can see the coupling coefficient decreases and the damping rates of both oscillators increase when graphene is coated. This implies that graphene impairs the coupling among the SRRs and decreases the Q factor of the resonance. When the graphene conductivity is decreased due to the intense THz field, increasing of the coupling coefficient and decreasing of damping rates are observed, leading to enhanced resonances.

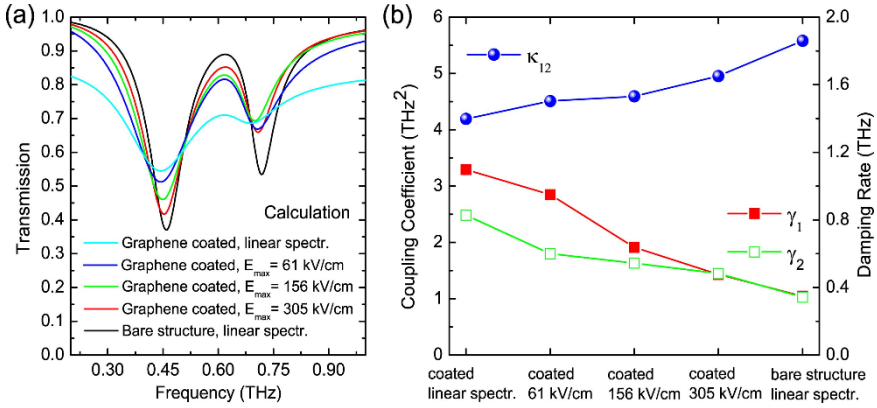

Fig. 6. (a) Calculated THz transmission spectra of the sample without graphene coating and with graphene coating under different THz field strengths. (b) The fitting parameters used in the corresponding calculations.

Optics EXPRESS

4. Conclusion

THz field induced transmission modulation of a graphene-metal hybrid metamaterial has been experimentally demonstrated. A modulation depth of 23% has been achieved at the transmission window (0.6 THz) when the THz field strength reached 305 kV/cm. This is much larger than the 4% transmission modulation observed for monolayer graphene on sapphire substrate. Simulations and mode analysis show that magneto-inductive and conductive couplings give rise to antisymmetric and symmetric modes in the graphene-metal hybrid metamaterial. The graphene coating with high conductivity impairs the two modes by weakening the coupling between them and increasing their damping rates. The high-field THz pulse leads to a decrease in graphene conductivity and helps to restore the strong resonance of the modes. Our study paves the way towards the design of tunable functional metamaterials integrated with graphene.

Funding

National Key Research and Development Program of China (2017YFA0701004); National Natural Science Foundation of China (NSFC) (61775159, 61735012, 61420106006, 61427814, 61875150, 61805129, 61605143); National Research, Development and Innovation Office (NKFIH) (2018-1.2.1-NKP-2018-00009, NN 125808)

References

1. H. T. Chen, A. J. Taylor, and N. Yu, "A review of metasurfaces: physics and applications," Rep. Prog. Phys. **79**(7), 076401 (2016).
2. N. Yu and F. Capasso, "Flat optics with designer metasurfaces," Nat. Mater. **13**(2), 139–150 (2014).
3. M. R. Hashemi, S. Cakmakyapan, and M. Jarrahi, "Reconfigurable metamaterials for terahertz wave manipulation," Rep. Prog. Phys. **80**(9), 094501 (2017).
4. J. He and Y. Zhang, "Metasurfaces in terahertz waveband," J. Phys. D Appl. Phys. **50**(46), 464004 (2017).
5. G. R. Keiser, K. Fan, X. Zhang, and R. D. Averitt, "Towards dynamic, tunable, and nonlinear metamaterials via near field interactions: a review," J. Infrared Millim. Terahertz Waves **34**(11), 709–723 (2013).
6. R. Singh, C. Rockstuhl, F. Lederer, and W. Zhang, "The impact of nearest neighbor interaction on the resonances in terahertz metamaterials," Appl. Phys. Lett. **94**(2), 021116 (2009).
7. S. Zhang, D. A. Genov, Y. Wang, M. Liu, and X. Zhang, "Plasmon-induced transparency in metamaterials," Phys. Rev. Lett. **101**(4), 047401 (2008).
8. Q. Xu, X. Su, C. Ouyang, N. Xu, W. Cao, Y. Zhang, Q. Li, C. Hu, J. Gu, Z. Tian, A. K. Azad, J. Han, and W. Zhang, "Frequency-agile electromagnetically induced transparency analogue in terahertz metamaterials," Opt. Lett. **41**(19), 4562–4565 (2016).
9. M. Liu, Z. Tian, X. Zhang, J. Gu, C. Ouyang, J. Han, and W. Zhang, "Tailoring the plasmon-induced transparency resonances in terahertz metamaterials," Opt. Express **25**(17), 19844–19855 (2017).
10. M. Liu, Q. Yang, Q. Xu, X. Chen, Z. Tian, J. Gu, C. Ouyang, X. Zhang, J. Han, and W. Zhang, "Tailoring mode interference in plasmon-induced transparency metamaterials," J. Phys. D Appl. Phys. **51**(17), 174005 (2018).
11. P. Weis, J. L. Garcia-Pomar, R. Beigang, and M. Rahm, "Hybridization induced transparency in composites of metamaterials and atomic media," Opt. Express **19**(23), 23573–23580 (2011).
12. D. J. Shelton, I. Brener, J. C. Ginn, M. B. Sinclair, D. W. Peters, K. R. Coffey, and G. D. Boreman, "Strong coupling between nanoscale metamaterials and phonons," Nano Lett. **11**(5), 2104–2108 (2011).
13. Q. Li, L. Cong, R. Singh, N. Xu, W. Cao, X. Zhang, Z. Tian, L. Du, J. Han, and W. Zhang, "Monolayer graphene sensing enabled by the strong Fano-resonant metasurface," Nanoscale **8**(39), 17278–17284 (2016).
14. W. Xu, L. Xie, and Y. Ying, "Mechanisms and applications of terahertz metamaterial sensing: a review," Nanoscale **9**(37), 13864–13878 (2017).
15. G. R. Keiser, N. Karl, P. Liu, C. Tulloss, H.-T. Chen, A. J. Taylor, I. Brener, J. L. Reno, and D. M. Mittleman, "Nonlinear terahertz metamaterials with active electrical control," Appl. Phys. Lett. **111**(12), 121101 (2017).
16. H. Cai, S. Chen, C. Zou, Q. Huang, Y. Liu, X. Hu, Z. Fu, Y. Zhao, H. He, and Y. Lu, "Multifunctional hybrid metasurfaces for dynamic tuning of terahertz waves," Adv. Opt. Mater. **6**(14), 1800257 (2018).
17. H. Liu, J. Lu, and X. R. Wang, "Metamaterials based on the phase transition of VO_2," Nanotechnology **29**(2), 024002 (2018).
18. M. Manjappa, Y. K. Srivastava, L. Cong, I. Al-Naib, and R. Singh, "Active photoswitching of sharp fano resonances in THz metadevices," Adv. Mater. **29**(3), 1603355 (2017).
19. J. Gu, R. Singh, X. Liu, X. Zhang, Y. Ma, S. Zhang, S. A. Maier, Z. Tian, A. K. Azad, H. T. Chen, A. J. Taylor, J. Han, and W. Zhang, "Active control of electromagnetically induced transparency analogue in terahertz metamaterials," Nat. Commun. **3**(1), 1151 (2012).

Optics EXPRESS

20. L. Cong, Y. K. Srivastava, H. Zhang, X. Zhang, J. Han, and R. Singh, "All-optical active THz metasurfaces for ultrafast polarization switching and dynamic beam splitting," Light Sci. Appl. **7**(1), 28 (2018).
21. X. Zhao, J. Zhang, K. Fan, G. Duan, G. D. Metcalfe, M. Wraback, X. Zhang, and R. D. Averitt, "Nonlinear terahertz metamaterial perfect absorbers using GaAs [Invited]," Photon. Res. **4**(3), A16–A21 (2016).
22. Y. K. Srivastava, M. Manjappa, L. Cong, H. N. S. Krishnamoorthy, V. Savinov, P. Pitchappa, and R. Singh, "A superconducting dual-channel photonic switch," Adv. Mater. **30**(29), 1801257 (2018).
23. M. Manjappa, Y. K. Srivastava, A. Solanki, A. Kumar, T. C. Sum, and R. Singh, "Hybrid lead halide perovskites for ultrasensitive photoactive switching in terahertz metamaterial devices," Adv. Mater. **29**(32), 1605881 (2017).
24. W. X. Lim, M. Manjappa, Y. K. Srivastava, L. Cong, A. Kumar, K. F. MacDonald, and R. Singh, "Ultrafast all-optical switching of germanium-based flexible metaphotonic devices," Adv. Mater. **30**(9), 1705331 (2018).
25. M. Manjappa, P. Pitchappa, N. Singh, N. Wang, N. I. Zheludev, C. Lee, and R. Singh, "Reconfigurable MEMS Fano metasurfaces with multiple-input-output states for logic operations at terahertz frequencies," Nat. Commun. **9**(1), 4056 (2018).
26. Q. Li, Z. Tian, X. Zhang, R. Singh, L. Du, J. Gu, J. Han, and W. Zhang, "Active graphene-silicon hybrid diode for terahertz waves," Nat. Commun. **6**(1), 7082 (2015).
27. B. Sensale-Rodriguez, R. Yan, M. M. Kelly, T. Fang, K. Tahy, W. S. Hwang, D. Jena, L. Liu, and H. G. Xing, "Broadband graphene terahertz modulators enabled by intraband transitions," Nat. Commun. **3**(1), 780 (2012).
28. B. Sensale-Rodriguez, R. Yan, S. Rafique, M. Zhu, W. Li, X. Liang, D. Gundlach, V. Protasenko, M. M. Kelly, D. Jena, L. Liu, and H. G. Xing, "Extraordinary control of terahertz beam reflectance in graphene electro-absorption modulators," Nano Lett. **12**(9), 4518–4522 (2012).
29. S. Xiao, T. Wang, T. Liu, X. Yan, Z. Li, and C. Xu, "Active modulation of electromagnetically induced transparency analogue in terahertz hybrid metal-graphene metamaterials," Carbon **126**, 271–278 (2018).
30. Z. Zhang, J. Yang, X. He, Y. Han, J. Zhang, J. Huang, D. Chen, and S. Xu, "Active control of broadband plasmon-induced transparency in a terahertz hybrid metal-graphene metamaterial," RSC Advances **8**(49), 27746–27753 (2018).
31. R. Degl'Innocenti, D. S. Jessop, Y. D. Shah, J. Sibik, J. A. Zeitler, P. R. Kidambi, S. Hofmann, H. E. Beere, and D. A. Ritchie, "Low-bias terahertz amplitude modulator based on split-ring resonators and graphene," ACS Nano **8**(3), 2548–2554 (2014).
32. F. Valmorra, G. Scalari, C. Maissen, W. Fu, C. Schönenberger, J. W. Choi, H. G. Park, M. Beck, and J. Faist, "Low-bias active control of terahertz waves by coupling large-area CVD graphene to a terahertz metamaterial," Nano Lett. **13**(7), 3193–3198 (2013).
33. S. H. Lee, M. Choi, T.-T. Kim, S. Lee, M. Liu, X. Yin, H. K. Choi, S. S. Lee, C.-G. Choi, S.-Y. Choi, X. Zhang, and B. Min, "Switching terahertz waves with gate-controlled active graphene metamaterials," Nat. Mater. **11**(11), 936–941 (2012).
34. T. T. Kim, H. Kim, M. Kenney, H. S. Park, H. D. Kim, B. Min, and S. Zhang, "Amplitude modulation of anomalously refracted terahertz waves with gated-graphene metasurfaces," Adv. Opt. Mater. **6**(1), 1700507 (2018).
35. T. T. Kim, H. D. Kim, R. Zhao, S. S. Oh, T. Ha, D. S. Chung, Y. H. Lee, B. Min, and S. Zhang, "Electrically tunable slow light using graphene metamaterials," ACS Photonics **5**(5), 1800–1807 (2018).
36. S. J. Kindness, N. W. Almond, B. Wei, R. Wallis, W. Michailow, V. S. Kamboj, P. Braeuninger-Weimer, S. Hofmann, H. E. Beere, D. A. Ritchie, and R. Degl'Innocenti, "Active control of electromagnetically induced transparency in a terahertz metamaterial array with graphene for continuous resonance frequency tuning," Adv. Opt. Mater. **6**(21), 1800570 (2018).
37. H. Jung, J. Koo, E. Heo, B. Cho, C. In, W. Lee, H. Jo, J. H. Cho, H. Choi, M. S. Kang, and H. Lee, "Electrically controllable molecularization of terahertz meta-atoms," Adv. Mater. **30**(31), e1802760 (2018).
38. M. J. Paul, Y. C. Chang, Z. J. Thompson, A. Stickel, J. Wardini, H. Choi, E. D. Minot, B. Hou, J. A. Nees, T. B. Norris, and Y.-S. Lee, "High-field terahertz response of graphene," New J. Phys. **15**(8), 085019 (2013).
39. H. Y. Hwang, N. C. Brandt, H. Farhat, A. L. Hsu, J. Kong, and K. A. Nelson, "Nonlinear THz conductivity dynamics in P-type CVD-grown graphene," J. Phys. Chem. B **117**(49), 15819–15824 (2013).
40. M. J. Paul, B. Lee, J. L. Wardini, Z. J. Thompson, A. D. Stickel, A. Mousavian, H. Choi, E. D. Minot, and Y.-S. Lee, "Terahertz induced transparency in single-layer graphene," Appl. Phys. Lett. **105**(22), 221107 (2014).
41. X. Li, Y. Zhu, W. Cai, M. Borysiak, B. Han, D. Chen, R. D. Piner, L. Colombo, and R. S. Ruoff, "Transfer of large-area graphene films for high-performance transparent conductive electrodes," Nano Lett. **9**(12), 4359–4363 (2009).
42. H.-L. Liu, S. Siregar, E. H. Hasdeo, Y. Kumamoto, C.-C. Shen, C.-C. Cheng, L.-J. Li, R. Saito, and S. Kawata, "Deep-ultraviolet Raman scattering studies of monolayer graphene thin films," Carbon **81**, 807–813 (2015).
43. M. Bruna, A. K. Ott, M. Ijäs, D. Yoon, U. Sassi, and A. C. Ferrari, "Doping dependence of the Raman spectrum of defected graphene," ACS Nano **8**(7), 7432–7441 (2014).
44. J. Hebling, G. Almási, I. Kozma, and J. Kuhl, "Velocity matching by pulse front tilting for large area THz-pulse generation," Opt. Express **10**(21), 1161–1166 (2002).
45. J. A. Fülöp, L. Pálfalvi, G. Almási, and J. Hebling, "Design of high-energy terahertz sources based on optical rectification," Opt. Express **18**(12), 12311–12327 (2010).
46. G. Sharma, I. Al-Naib, H. Hafez, R. Morandotti, D. G. Cooke, and T. Ozaki, "Carrier density dependence of the nonlinear absorption of intense THz radiation in GaAs," Opt. Express **20**(16), 18016–18024 (2012).

Optics EXPRESS

47. N. Liu, S. Kaiser, and H. Giessen, "Magnetoinductive and electroinductive coupling in plasmonic metamaterial molecules," Adv. Mater. **20**(23), 4521–4525 (2008).
48. N. Liu and H. Giessen, "Coupling effects in optical metamaterials," Angew. Chem. Int. Ed. Engl. **49**(51), 9838–9852 (2010).
49. J. M. Dawlaty, S. Shivaraman, M. Chandrashekhar, F. Rana, and M. G. Spencer, "Measurement of ultrafast carrier dynamics in epitaxial graphene," Appl. Phys. Lett. **92**(4), 042116 (2008).
50. H. J. Shin, J. Kim, S. Kim, H. Kim, V. L. Nguyen, Y. H. Lee, S. C. Lim, and J.-H. Son, "Transient carrier cooling enhanced by grain boundaries in graphene monolayer," ACS Appl. Mater. Interfaces **9**(46), 41026–41033 (2017).
51. I. Maeng, S. Lim, S. J. Chae, Y. H. Lee, H. Choi, and J. H. Son, "Gate-controlled nonlinear conductivity of Dirac fermion in graphene field-effect transistors measured by terahertz time-domain spectroscopy," Nano Lett. **12**(2), 551–555 (2012).
52. H. A. Hafez, P. L. Levesque, I. Al-Naib, M. M. Dignam, X. Chai, S. Choubak, P. Desjardins, R. Martel, and T. Ozaki, "Intense terahertz field effects on photoexcited carrier dynamics in gated graphene," Appl. Phys. Lett. **107**(25), 251903 (2015).